Characterization of Nicergoline Polymorphs Crystallized in Several Organic Solvents

LEDJAN MALAJ,[1,2] ROBERTA CENSI,[1,3] DORETTA CAPSONI,[4] LUCA PELLEGRINO,[5] MARCELLA BINI,[4] STEFANIA FERRARI,[4] ROBERTO GOBETTO,[5] VINCENZO MASSAROTTI,[4] PIERA DI MARTINO[1]

[1]University of Camerino, School of Pharmacy, Camerino, Italy

[2]University of Tirana, Department of Pharmacy, Rr. Dibres, Tirana, Albania

[3]Department of Pharmaceutics, Utrecht Institute for Pharmaceutical Sciences, Utrecht University, Utrecht, the Netherlands

[4]Department of Physical Chemistry, University of Pavia, "M. Rolla", Pavia, Italy

[5]Department of Chemistry I.F.M., University of Turin, Turin, Italy

Received 13 September 2010; revised 9 December 2010; accepted 14 December 2010

Published online 19 January 2011 in Wiley Online Library (wileyonlinelibrary.com). DOI 10.1002/jps.22477

ABSTRACT: Nicergoline (NIC), a poorly water-soluble semisynthetic ergot derivative, was crystallized from several organic solvents, obtaining two different polymorphic forms, the triclinic form I and the orthorhombic form II. NIC samples were then characterized by several techniques such as ^{13}C cross-polarization magic angle spinning solid-state spectroscopy, room-temperature and high-temperature X-ray powder diffraction, differential scanning calorimetry, and by analysis of weight loss, solvent content, powder density, morphology, and particle size. Solubility and intrinsic dissolution rates determined for the two polymorphic forms in water and hydrochloride solutions (HCl 0.1 N) were always higher for form II than for form I, which is actually the form used for the industrial preparation of NIC medicinal products. Preformulation studies might encourage industry for the evaluation of polymorph II, as it is more suitable for pharmaceutical applications. Results in drug delivery, as well as those obtained by the above-mentioned techniques, and the application of Burger–Ramberger's rules make it possible to conclude that there is a thermodynamic relation of monotropy between the two polymorphs. This last assumption may help formulators in predicting the relative stability of the two forms.
 J Pharm Sci 100:2610–2622, 2011

Keywords: nicergoline; polymorphism; monotropy; solid state NMR ; thermal analysis; solubility; dissolution

INTRODUCTION

Poorly water-soluble drugs are associated with slow drug absorption, which can lead to inadequate and variable bioavailability.[1,2] Currently, nearly 40% of the new chemical entities being discovered are poorly water-soluble drugs.[3]

An enhancement of drug solubility of therapeutic agents can possibly improve their bioavailability. Most formulation strategies for poorly water-soluble drugs seek to improve their dissolution rate and/or solubility *in vivo* by achieving different polymorphic forms,[4–6] solvates, or hydrates,[7] amorphous forms,[8] complexes such as drug–cyclodextrins,[9,10] or solid dispersions of drugs in hydrophilic polymers.[11]

This study considers in depth the polymorphic forms of NIC with particular emphasis on their physicochemical stability, solubility, and dissolution rates.

NIC [10α-methoxy-1,6-dimethylergoline-8β-methanol-5′-bromonicotinate ($C_{24}H_{26}BrN_3O_3$)] is a semisynthetic ergot derivative (Fig. 1) that is water insoluble in its crystalline state. NIC is a potent blocking agent for α1-adrenoreceptors and thus has found effective clinical use in neurology,[12] particularly improving cerebral blood flow and being effective in senile dementia. In addition, it shows remarkable effects in lowering systemic blood pressure and dilating blood vessels, thereby increasing

Correspondence to: Piera Di Martino (Telephone: +39-0737-4022-15; Fax: +39-0737-6373-45; E-mail: piera.dimartino@unicam.it)

Journal of Pharmaceutical Sciences, Vol. 100, 2610–2622 (2011)

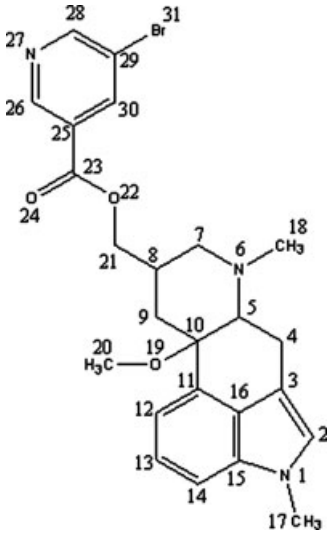

Figure 1. Molecular structure of nicergoline.

peripheral blood flow.[13] NIC has also been clinically used for improving metabolism in the brain, particularly for treatment of senile dementia.[14] The drug has proved to have cerebral anti-ischemic action, also exhibiting platelet antiaggregation and disaggregating actions.[15,16] Several clinical studies have demonstrated that NIC is effective in lowering total peripheral resistance and normalizing blood pressure without producing reflex tachycardia, and concluded that the drug is useful in the early phases of acute myocardial infarction due to its lowering of myocardial oxygen consumption.[17]

NIC may exist in two different polymorphic forms:

(a) Form I crystallizes in the triclinic $P1$ space group (s.g.), with $a = 7.729$ Å, $b = 8.695$ Å, $c = 17.030$ Å, $\alpha = 100.90^\circ$, $\beta = 98.67^\circ$, $\gamma = 93.04^\circ$, $Z = 2$.[18]

(b) Form II belongs to the orthorhombic $P2_12_12_1$ s.g., with $a = 11.507$ Å, $b = 13.219$ Å, $c = 14.753$ Å, $Z = 4$.[19,20] The purpose of this study was to characterize different samples of NIC crystallized in several organic solvents by several methods. There is limited literature on the full characterization of NIC, hence the focus of the study. The relative thermodynamic stability of forms I and II according to Burger–Ramberger's rules[21] will be discussed and evaluated. Solubility and dissolution profiles of the two polymorphic forms will also be assessed.

MATERIALS AND METHODS

Materials

Nicergoline United States Pharmacopeia (USP) was purchased from China-Japan Shandong Hongfuda Pharmchem Co., Ltd. (Shandong, China). This sample, used in its native form, will be indicated as reference NIC (REF-NIC). The analytical grade solvents used for the study were ethyl acetate (ETA), acetone (ACE), acetonitrile (ACN), dichloromethane (DCM), tetrahydrofurane (THF), and ethanol [ETH (98%)]. The samples crystallized in these solvents, for sake of simplicity, will be indicated as ETA–NIC, ACE–NIC, ACN–NIC, DCM–NIC, THF–NIC, and ETH–NIC, respectively.

Crystallization

The crystalline samples were obtained by the cooling crystallization method. Supersaturation was achieved by changing the solution temperature. A predetermined drug amount, able to form a saturated solution at room temperature (RT), was dissolved in a particular solvent volume at 40.0 ± 0.5°C, and the solution was cooled at 10°C under continuous stirring by means of an external ethanol cooling system (Cryostat F4-Q; Haake Q, Karlsruhe, Germany). Crystals were recovered by vacuum filtration, dried at RT for 24 h in a ventilated oven, and then stored at 25.0 ± 0.5°C in a desiccator. Crystals were not sieved.

Scanning Electron Microscopy

Nicergoline crystal morphology was determined using a scanning electron microscope (Stereoscan 360; Cambridge Instruments, Cambridge, United Kingdom). Samples were mounted on a metal stub with double-sided adhesive tape and then sputtered under vacuum with a gold layer of about 200-Å thickness using a metallizator (Oerlikon Balzers MED 010; Milan, Italy).

Particle size was determined by measuring the Ferret's diameter of 500 particles.

Helium Pycnometry

The powder density was determined using a helium pycnometer (Accupyc 1330; Micromeritics, Norwolk, Connecticut) with a cell of 10 cm^3. Results are the mean of 10 measurements.

Data were analyzed by one-way analysis of variance (ANOVA), using the Bonferroni test. The statistical analysis was conducted using an Origin® Pro software (version 8.5); OriginLab Corporation, Northampton, MA, USA).

Simultaneous Thermal Analysis

Simultaneous thermal analysis (STA) allowed simultaneous analysis of thermogravimetric analysis (TGA) and differential scanning calorimetry (DSC). In this text, the acronym TGA–STA refers to TGA obtained from STA. The analysis was performed with a simultaneous thermal analyzer (STA 6000; PerkinElmer, Inc., Waltham, Massachusetts), under nitrogen atmosphere (20 mL/min) in 0.07 mL open

aluminum oxide pans. STA was calibrated for temperature and heat flow with three standard metals (tin, indium, and zinc), taking into account their expected melting temperatures (505.08, 429.75, and 692.68 K, respectively), and for weight with an external PerkinElmer standard (calibration reference weight P/N N520-0042, material lot #91101 GB, weight 55.98 mg, 01/23/08 VT). Calibration was repeatedly checked to assure deviation of ±0.3 K. The analysis was performed (approximately 10 mg of sample) in quadruplicate by heating from 20°C to 150°C at a heating rate of 5°C/min. The weight loss was determined between 20°C and 100°C. STA was mainly used for TGA analysis. For DSC study, a different apparatus, described in the next paragraph, was preferred for its higher sensitivity in the evaluation of enthalpy change at the melting interval.

Differential Scanning Calorimetry

Differential scanning calorimetry analysis was performed on a Pyris 1 apparatus (PerkinElmer, Co.) equipped with a cooling device (Intracooler 2P, Cooling Accessory; PerkinElmer, Co.). A purge of dry nitrogen gas (20 mL/min) was used for all runs. DSC was calibrated for temperature and heat flow using a pure sample of indium and zinc as standards, following the same criteria previously described for STA. Sample mass was about 3–4 mg and aluminum perforated pans were used. Each run was performed in triplicate from 0°C to 150°C at different heating rates: 1.0 and 10.0°C/min. To avoid confusion with DSC–STA results, this technique will be identified as conventional DSC.

X-Ray Powder Diffraction

The RT and high-temperature (HT) X-ray powder diffraction (XRPD) data were collected in static air by means of a Bruker D5005 diffractometer (Bruker AXS, Karlsruhe, Germany) equipped with an Anton Paar TTK450 polythermal attachment with the Cu Ka radiation (l_{a1} = 1.54056 Å, l_{a2} = 1.54430 Å). A Ni filter and a position-sensitive detector were used. The patterns were collected in step-scan mode in the angular range of 5–35°/2q, step 0.015°, and 0.3 s/step; at RT, 100°C, 110°C, and 130°C; and at RT after cooling (heating rate 1°C/min; spontaneous cooling). For the sample crystallized from THF, additional measurements were performed by (i) changing the heating and cooling rate or adding isothermal steps at 125°C, to explore how kinetics may influence the transition; (ii) making use of a N2 flow during measurements, to possibly prevent sample decomposition and to better reproduce the experimental conditions used in the thermal measurements. A detailed analysis of the crystalline polymorphs, structure, and phase abundance (wt %) in the cases of multiphase samples can be carried out by means of the structural and profile refinement of the experimental pattern on the basis of the Rietveld method. This approach allows to refine a series of structural (such as lattice parameters, atoms position, thermal factors, and site occupancies) and profile parameters by minimizing the difference between the observed and calculated pattern. The calculated one is obtained by the structural data known in literature, in our case the forms I and II crystal structures.[18–20] The Rietveld structural and profile refinement were carried out by means of TOPAS V3.0 software.[21]

High-Resolution ^{13}c Solid-State NMR Spectroscopy

^{13}C cross-polarization magic angle spinning (CP-MAS) spectra of the different samples were run on a Bruker Avance II instrument operating at 100.64 MHz for ^{13}C nuclei. Cylindrical 4-mm (o.d.) zirconia rotors with a sample volume of 120 μL were employed. For all samples, the magic angle was carefully adjusted from the ^{79}Br spectrum of KBr by minimizing the line width of the spinning sideband satellite transitions. Samples were spun at 12 kHz at RT. A ramp cross-polarization pulse sequence was used with a contact time of 3 ms, recycle delays of 5 s, and 600–2000 transients. ^{13}C chemical shifts were referenced with the resonance of solid hexamethylbenzene (^{13}C methyl signal at d = 17.4 ppm).

Gas-Phase Chromatography

The determination of solvent content in the samples was performed by gas-phase chromatography (GPC) according to the USP method (27–467 organic volatile impurities) on an Agilent Shimadzu GC-14B chromatograph (Agilent Technologies, Waldbronn, Germany) fitted with a flame ionization detector. The packed column was a DB-624, 30 m × 3.0 mm; carrier gas was helium (constant flow, 35 cm/s). The oven was heated from 40°C to 250°C at 30°C/min. For assay, a certain amount of NIC was dissolved in 5 mL ethanol to obtain a solution having a known concentration of about 20 mg/mL, which was then injected into the chromatograph.

Equilibrium Solubility in Water Solutions

An excess of drug powder was added to 50 mL of water or HCl 0.1 N and maintained at four different temperatures (10, 20, 30, and 40 ± 0.5°C) under continuous stirring in an incubator (FTC 90E; Velp Scientifica, Usmate, Italy). Equilibrium was tested and judged to have been reached when three successive measurements differed by no more than 1%, generally after 24 h. After equilibrium was reached, aliquots were taken, filtered with a regenerated cellulose filter syringe of 0.45-mm pore size (Filalbet; Rossello, Barcelona, Spain), and, after appropriate dilution, the concentration of the filtrate was determined by ultraviolet spectrophotometer at a wavelength of 288 nm

(Cary 1E UV-VIS; Varian, Leinì, Italy). Assays were performed in triplicate.

Intrinsic Dissolution Rate Study

Dissolution study was carried out by the rotating disk method.[22] Approximately 13-mm diameter tablets were obtained by compressing 300 mg of powder using a PerkinElmer hydraulic press for KBr disks for infrared spectroscopy, at a force of 15 kN for 10 min. This yielded tablets with a surface area of 132.73 mm^2 that would not disintegrate during the test. Tablets were inserted into a stainless steel holder, so that only one face was exposed to the dissolution medium. The holder was then connected to a stirring motor, centrally immersed in a 1000-mL beaker containing 900 mL of demineralized water or HCl (0.1 N) at 37°C and rotated at 50 rpm. Suitable aliquots were withdrawn with a regenerated cellulose filter syringe at specified times and assayed for drug content spectrophotometrically at a wavelength of 288 nm. A correction was calculated for cumulative dilution caused by replacement of the sample with an equal volume of original medium. Each test was repeated six times. Low standard deviations were obtained, indicating the good reproducibility of this technique. Data were analyzed by one-way ANOVA, using the Bonferroni test. The statistical analysis was conducted using an Origin® software (version 8.5).

The intrinsic dissolution rates (IDRs) were calculated from the slope of the straight line of cumulative drug release.

RESULTS AND DISCUSSION

Physicochemical Properties

The physicochemical properties of NIC crystallized in different organic solvents are shown in Table 1. The low weight loss percentage determined by TGA–STA for all the samples reveals that no solvated forms were produced after crystallization in the different solvents. These results are in agreement with the solvent content determined by GPC, which was low and rather homogeneous among all the samples. GPC also revealed a high degree of purity of the investigated samples.

Powder Densities

These were determined by helium pycnometry and are shown in Table 1. The powder densities of REF–NIC and ETA–NIC samples were always higher than those of powders crystallized from the other solvents. The ANOVA test indicates that powder densities of REF–NIC and ETA–NIC were significantly different from those of forms obtained from the other solvent ($p < 0.05$). Densities of powders crystallized from the other solvents were not statistically different (significance level $p > 0.05$) This may suggest that both REF–NIC and ETA–NIC samples have similar molecular packing, different from that of the other samples.

Particles Morphology

Figure 2 shows scanning electron microscopy (SEM) microphotographs of the samples. To compare crystal morphology, the same magnification was used (1.5k×). In spite of clear differences in particle size, the particle shape was similar. Crystals appeared as irregular particles with sharp edges. The mean particle diameter is shown in Table 1, and as clearly evident from SEM microphotographs, it was quite different among all the samples. Broad and nonhomogeneous particle size distribution was also confirmed by the high standard deviations (Table 1).

Table 1. Physicochemical Properties of Nicergoline Samples Crystallized from Different Solvents

Nicergoline Samples	Weight Loss (%)[a]	Solvent Content (ppm)[b]	Powder Density (g/cm^3)[c]	Mean Particle Diameter (μm)[d]	Melting Peak[e]	
					T_{onset} (°C)	ΔH (J/g)
REF–NIC	0.12 ± 0.10	34.0 ± 2.8	1.4001 ± 0.0001	4.76 ± 4.09	134.9 ± 2.1	58.4 ± 5.2
ETA–NIC	0.20 ± 0.16	46.3 ± 4.1	1.4046 ± 0.0001	4.95 ± 2.14	134.2 ± 1.9	57.8 ± 4.9
ACE–NIC	0.58 ± 0.25	67.1 ± 5.0	1.3276 ± 0.0001	2.76 ± 1.76	120.2 ± 3.0	56.2 ± 5.2
ACN–NIC	0.47 ± 0.31	52.8 ± 6.0	1.3755 ± 0.0002	8.95 ± 6.43	122.6 ± 1.2, 136.2 ± 0.8	58.8 ± 8.2, 14.5 ± 2.3
DCM–NIC	0.36 ± 0.14	60.0 ± 5.2	1.3178 ± 0.0003	10.10 ± 7.10	121.5 ± 2.7	54.4 ± 4.5
ETH–NIC	0.33 ± 0.21	50.6 ± 3.7	1.3577 ± 0.0002	7.33 ± 6.81	120.8 ± 1.8	55.6 ± 6.7
THF–NIC	0.43 ± 0.15	52.4 ± 6.8	1.3670 ± 0.0001	5.43 ± 4.75	121.0 ± 2.5	57.9 ± 4.8

[a] Determined by TGA–STA between 20°C and 100°C.
[b] Determined by gas chromatography.
[c] Determined by helium pycnometry.
[d] Determined by measuring the Ferret's diameter of 500 particles observed through the SEM analysis.
[e] Determined by conventional DSC at the heating rate of 10°C/min.
REF, reference; NIC, nicergoline; ETA, ethyl acetate; ACE, acetone; ACN, acetonitrile; DCM, dichloromethane; ETH, ethanol; THF, tetrahydrofurane.

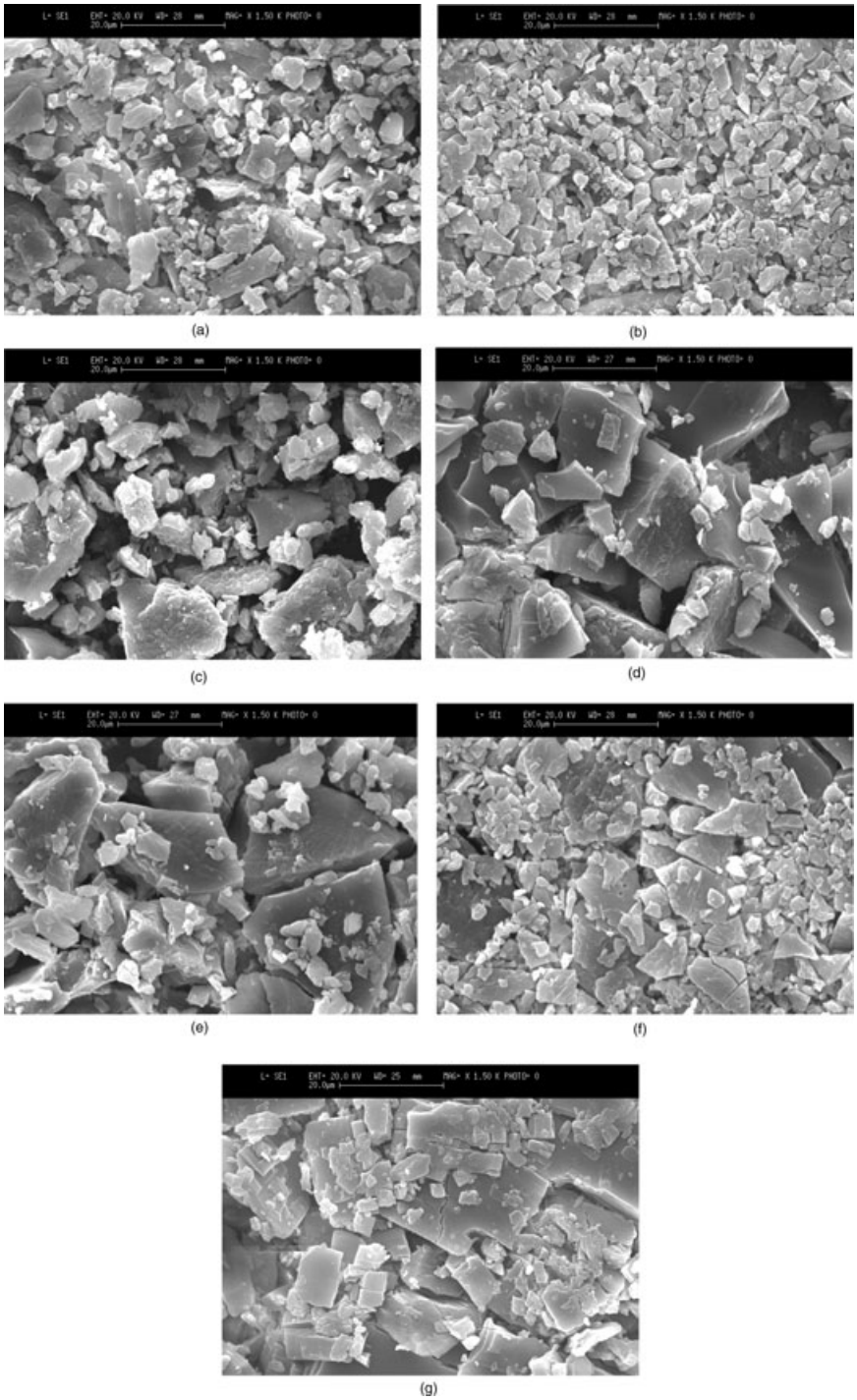

Figure 2. Scanning electron microscopy photomicrographs of the samples crystallized in different solvents. (Magnification = 1.5k×). (a) Ethyl acetate–nicergoline (NIC), (b) acetone–NIC, (c) acetonitrile–NIC, (d) dichloromethane–NIC, (e) ethanol–NIC, (f) tetrahydrofurane–NIC, and (g) reference–NIC.

X-Ray Powder Diffraction

The powder diffraction patterns of ETH–NIC, ACE–NIC, ACN–NIC, DCM–NIC, and THF–NIC samples were different with respect to that of REF–NIC (Fig. 3). The ETA–NIC pattern was instead quite comparable to that of REF–NIC. These results suggest that two different crystalline forms were obtained from the solvents considered for the study. The peaks present in REF–NIC and ETA–NIC are well explained by the triclinic structure (form I),[18] whereas peaks present in ACN–NIC, ACE–NIC, DCM–NIC,

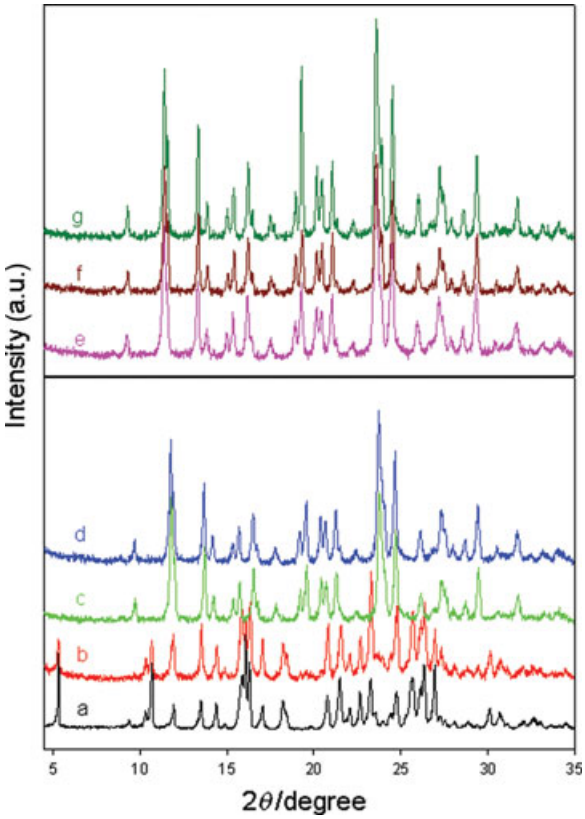

Figure 3. Room-temperature X-ray powder diffraction patterns of (a) reference–nicergoline (NIC), (b) ethyl acetate–NIC, (c) acetonitrile—NIC, (d) tetrahydrofurane–NIC, (e) dichloromethane–NIC, (f) ethanol–NIC, and (g) acetone–NIC.

THF–NIC, and ETH–NIC samples well matched the orthorhombic one (form II).[19,20] On the basis of the crystal structures for the two polymorphs reported in the literature,[18–20] the Rietveld refinement was carried out on all the samples. Satisfactory results were obtained for the samples having the orthorhombic structure. Both position and intensities of all the peaks of each pattern are completely explained by the form II structural model ($P2_12_12_1$ s.g.) As an example, the comparison between the observed and calculated pattern for the ACN–NIC sample is shown in Figure 4a; satisfactory discrepancy factors and goodness of fit (GoF) were obtained by refinement (Rwp = 11.16, GoF = 1.45). Also the structural refinement applied to the ETA–NIC diffraction data on the basis of triclinic $P1$ structure leads to good results (R_{wp} = 15.70, GoF = 2.26); a more detailed analysis highlighted the presence of small peaks belonging to the orthorhombic phase (angular regions: 13°, 18–21°, and 24°). The Rietveld structural refinement performed by taking into account the copresence of both polymorphic structures completely explains the experimental pattern and gives very satisfactory results (R_{wp} = 9.58, GoF = 1.40), evidenced also by the comparison between observed and calculated patterns shown in Figure 4b. The quantitative analysis obtained by the structural refinement leads to 91.5 (4) and 8.5(4) wt % of triclinic and orthorhombic phase, respectively.

^{13}c CP-MAS NMR

The ^{13}C CP-MAS NMR spectra of REF–NIC (a) and that of ETA–NIC (b) were superimposable, showing several split signals, according to the presence of two types of molecules in the same unit cell (Fig. 5 and Table 2). Conversely, samples c, d, f, and g showed the same ^{13}C spectra, with a number of resonances related to the presence of only one type of molecule in the unit cell. All resonances had different chemical shift values with respect to the REF–NIC (a) and the ETA–NIC (b). The chemical shifts observed in solution are related to the time-averaged, isotropic environments of the nuclei. Thus, it is possible to conclude that the NMR data are in perfect agreement with the XRPD results previously reported.

Additional analytical techniques are useful for consolidating the structural evidences and for fully characterizing the different forms from a physicochemical point of view.

Differential Scanning Calorimetry

Differential Scanning Calorimetry analysis confirmed the XRPD results, but also added new evidences

Table 2. Assignments and Chemical Shifts of Nicergoline Samples

Carbon Atoms	Group	REF–NIC ETA–NIC	ACE–NIC, ACN–NIC, DCM–NIC, ETH–NIC, THF–NIC
C4	CH_2	23.7	23.0
C9	CH_2	28.3	28.7
C18	CH_3	29.7	33.1
C8	CH	32.5	34.8
C17	CH_3	45.3	42.0
C20	CH_3	50.0	48.5
C7	CH_2	60.7	62.1
C21	CH_2	67.7	67.1
C5	CH	71.5	70.5
C10	C_q	74.8	74.7
C14	CH	110.1	109.3
C29, C3	C_q	111.4	112.0
C12	CH	115.6	114.9
C13	CH	121.7	122.4
C2	CH	124.9	124.8
C25, C16	C_q	127.3	127.5
C11	C_q	131.2	131.4
C15	C_q	136.7	136.2
C30	CH	138.9	138.4
C26, C28	CH	147.6	148.8
C26, C28	CH	152.9	157.9
C23	C=O	163.2	164.2

ACE, acetone; NIC, nicergoline; ACN, acetonitrile; DCM, dichloromethane; ETH, ethanol; THF, tetrahydrofurane.

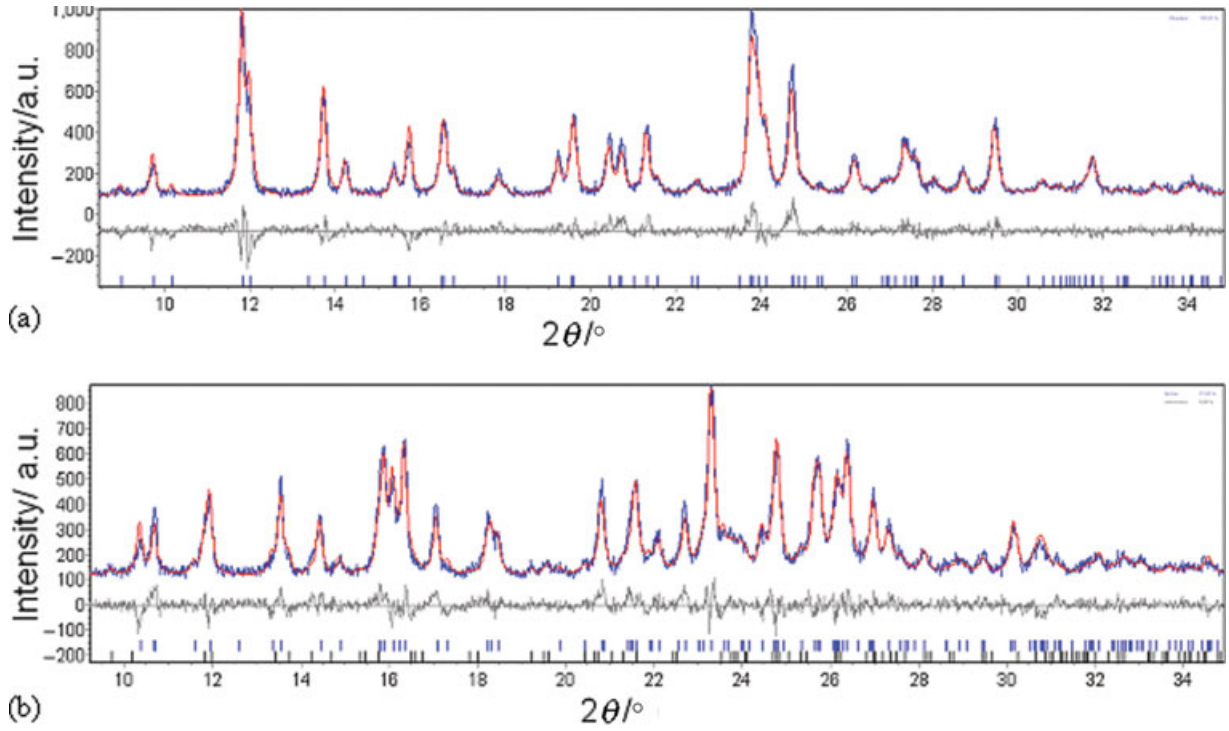

Figure 4. Observed (blue line) and calculated (red line) room-temperature X-ray powder diffraction pattern after Rietveld refinement of samples (a) acetonitrile–nicergoline (NIC) (orthorhombic form II) and (b) ethyl acetate–NIC (triclinic form I). At the bottom, the difference between observed and calculated patterns and the peak positions are also shown.

(Fig. 6 and Table 1). In particular, the thermograms differ depending on the crystallization solvent and the heating rate.

The thermograms of REF–NIC and ETA–NIC are identical, irrespective the heating rate, and they show one endothermic peak corresponding to the melting of the form I at nearly 134.0°C. This result confirms that the two samples correspond to the same crystalline form and in particular to the triclinic form I, as pointed out by XRPD and ^{13}C CP-MAS NMR. At 10°C/min, the thermograms of the ETH–NIC, ACE–NIC, DCM–NIC, and THF–NIC samples showed one endothermic peak at 120.0°C–122.0°C for all the samples, and thus presumably corresponding to the melting of polymorphic form II. At lower heating rate (1°C/min), in the case of the ACE–NIC, DCM–NIC, and THF–NIC samples, the first endothermic peak corresponding to the melting of form II was followed by a very low exotherm one, and then the melting of form I was observed. The ETH–NIC sample showed the melting of form II only. In the thermogram of the ACN–NIC sample, it was possible to observe the melting endothermic peak of form II, followed by the exotherm and then by the melting endothermic one of form I.

This behavior was the same whatever the heating rate. These results suggest a common thermal behavior of the samples crystallized in form II; the heating rate and the possible presence of small amounts of seeds of form I play a relevant role in evidencing the melting–recrystallization phenomena in the form II polymorph. The form I is the higher-melting polymorph and has slightly higher values of enthalpy of melting (Table 1). On the basis of the heat of fusion rule of Burger and Ramberger,[23] a monotropic relationship between the polymorphs can be suggested. This hypothesis is also supported by the absence of the transition between the two polymorphs before melting.

High-temperature XRPD

The measurements were made to clarify the relationship between the polymorphic forms and to characterize their thermal stability. The temperatures (100°C, 110°C, and 130°C and 25°C after spontaneous cooling) and heating rates were chosen on the basis of the DSC evidence.

The ETA–NIC sample shows comparable diffractograms, suggesting the stability of the form I polymorph up to 130°C (Fig. 7). The pattern collected at 100°C was not shown to make the figure less congested. Some differences could be observed in the peak positions, intensities, and splitting of the reflections between the RT and HT patterns due to the expansion of the lattice parameters of the triclinic cell with increasing temperatures, as demonstrated by the Rietveld structural refinement, which will be

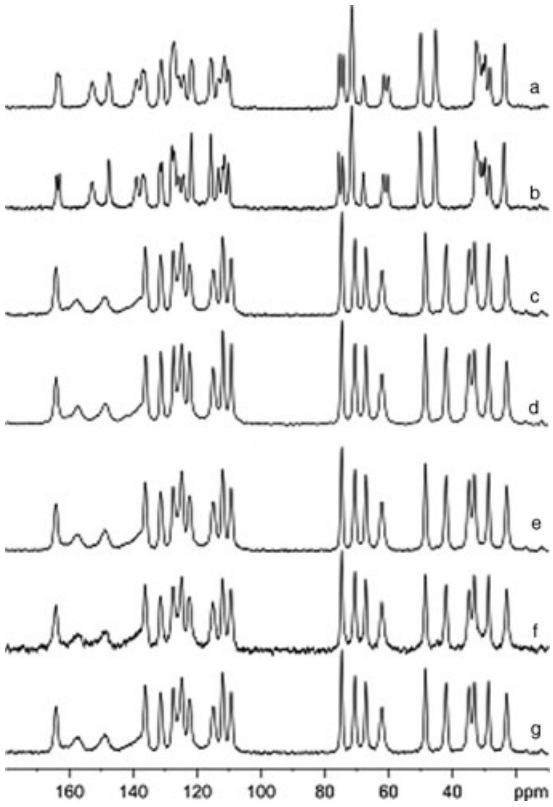

Figure 5. Comparison of ^{13}C cross-polarization magic angle spinning spectra of nicergoline samples: (a) reference–nicergoline (NIC), (b) ethyl acetate–NIC, (c) ethanol–NIC, (d) acetonitrile–NIC, (e) acetone–NIC, (f) dichloromethane–NIC, and (g) tetrahydrofurane–NIC.

discussed later. The diffractogram after cooling to RT (pattern d) was perfectly superimposable on the pattern a. The HT-XRPD results were in agreement with the DSC evidence, suggesting that the form I polymorph is fairly stable up to the melting point (about 134°C). The same thermal behavior was also observed for the REF–NIC.

The patterns of ACN–NIC (Fig. 8) collected at 100°C and 110°C showed the same reflections observed at RT, suggesting that the orthorhombic form II is stable at least up to 110°C. The patterns collected at 100°C were not shown in the figure for brevity. Further heating to 130°C leads to the structural transition of polymorph II to the polymorph I. The transition is irreversible as demonstrated by the pattern collected at RT after spontaneous cooling, which is actually comparable with that obtained at 130°C if the peak position shifts due to the thermal contraction of the lattice volume with cooling is taken into account. Our HT-XRPD data correlated well with the DSC results. Thus, the melting–crystallization peaks observed at 10 and 1°C/min at about 123°C may be attributed to the crystallization of the triclinic form. The orthorhombic form of THF–NIC patterns was stable at 110°C, similar to that of ACN–NIC (Fig. 9). The pattern collected at 130°C clearly shows that in the temperature range 110°C–130°C, the sample melts, in agreement with the DSC results (heating rate 10°C/min), evidencing an endothermic peak at 121°C. In contrast to the ACN–NIC, the sample did not recrystallize in the triclinic form but decomposed, as demonstrated by the presence of the main peak of graphitic carbon at about 26°/2q. After cooling, no crystallinity was recovered. The different thermal behaviors observed by XRPD for the same form II polymorph when crystallized by different solvents (ACN–NIC and THF–NIC) merited further inquiry.

Additional measurements were carried out by (i) changing the heating and cooling rate or adding isothermal steps at 125°C, to explore how kinetics may influence the transition; (ii) making use of a N2 flow during measurements, to possibly prevent sample decomposition and to better reproduce the experimental conditions used in the thermal measurements. No crystallization was observed when the diffractograms were collected at 120°C, 125°C after 2 h, and 128°C, nor was it seen when the heating (10°C/min) and cooling (1°C/min) rates were changed. Thus, the lack of crystallization did not seem to be due to kinetic reasons. The HT measurements performed in N_2 flow (HTK Anton Paar polythermal attachment, which can work in nonambient atmosphere) confirm the preservation of the orthorhombic form up to 110°C, after which the sample melts, as suggested by the pattern collected at 130°C. In this case, there was no evidence of decomposition or crystallization compared with measurements performed in air.

The thermal differences between ACN–NIC and THF–NIC could be explained by taking into account the possibility that the ACN–NIC sample might have a small amount of NIC in the triclinic form (a small percentage below the detection limit of the XRPD technique), which acts as a crystallization seed of the form I polymorph, when the orthorombic phase melts at about 124°C. From DSC results obtained with a low heating rate (1°C/min instead of 10°C/min), a weak peak of crystallization after form II melting at about 124°C and another weak melting peak at 134°C can be detected. This suggests that the THF–NIC orthorhombic form also transforms into the triclinic one, but this transition needed peculiar experimental conditions, similar to those used for the DSC measurements that cannot be reached by XRPD. The thermal behavior described for the THF–NIC was also observed for ETH–NIC, DCM–NIC, and ACE–NIC.

Rietveld Structural Refinement

The refinement performed on all the HT patterns allowed us to study the trend of the lattice parameters with temperature. The results are shown in Figure 10. For the ETA–NIC, the HT patterns were refined on the basis of the coexistence of the two

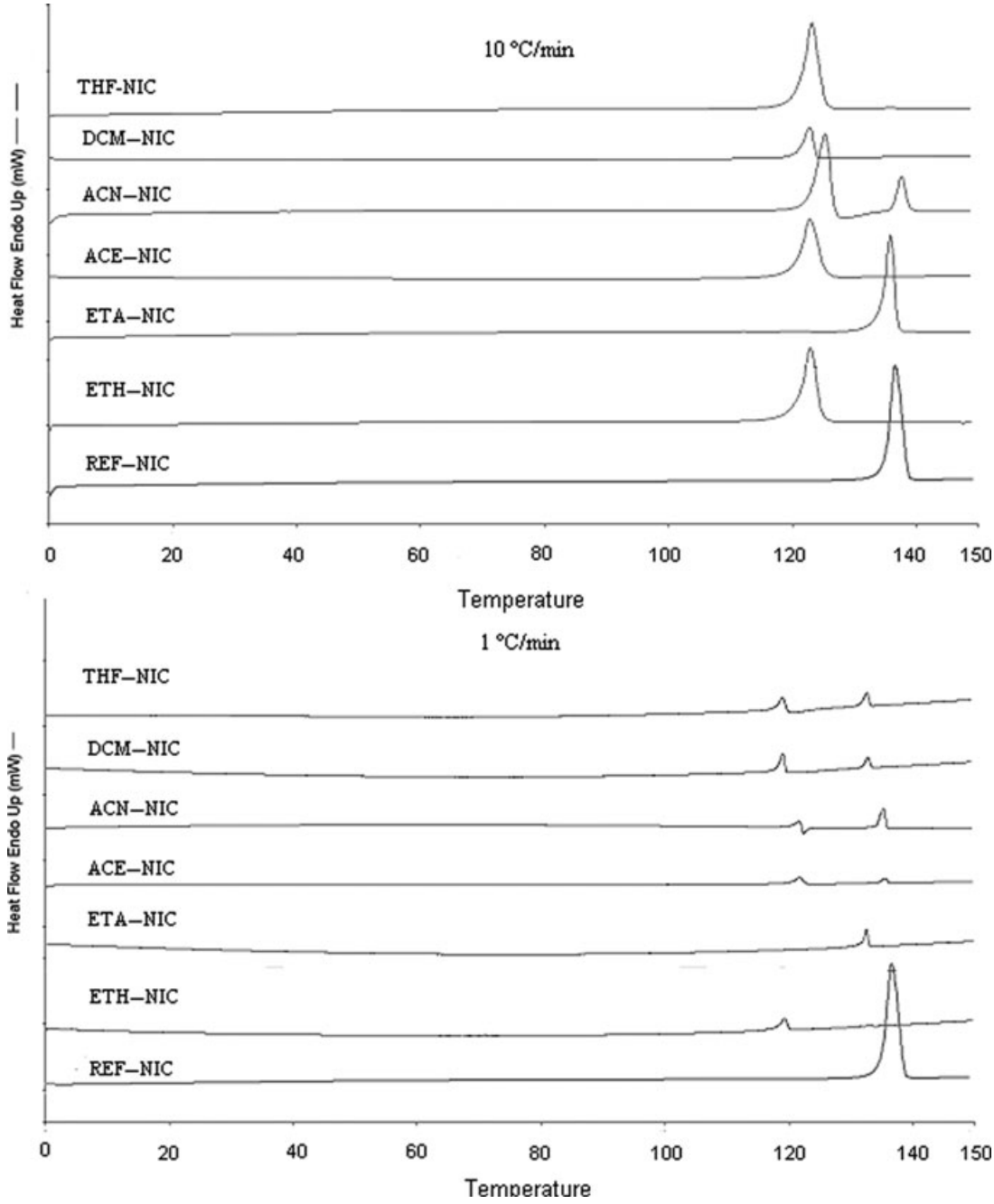

Figure 6. Differential scanning calorimetry thermograms of reference–nicergoline (NIC) and NIC crystallized from several solvents at different scanning rates (10 and 1°C/min).

crystallographic structures, and the two phases were quantified. The orthorhombic polymorph is present in 7.2(4) and 6.0(3) wt % for the sample at 100°C and 110°C, respectively; this amount agrees well with that already revealed in the sample at RT. In the pattern collected at 130°C, the two-phase model Rietveld refinement unambiguously suggests that there is only a triclinic *P*1 phase. This is in agreement with the evidence previously discussed, demonstrating that the orthorhombic phase is stable only up to about 124°C, and then melts or transforms to the triclinic form.

Equilibrium Solubility and Drug Release

Equilibrium solubility and drug release were tested for all the samples. Because the major differences were due to the crystallographic forms, for brevity only, results of REF–NIC for the form I and ETH–NIC for the form II are reported. Actually, it is necessary to clarify that both solubility and IDR are not influenced by other parameters such as particle size and distribution. The equilibrium solubility of forms I (REF–NIC) and II (ETH–NIC) in water and HCl

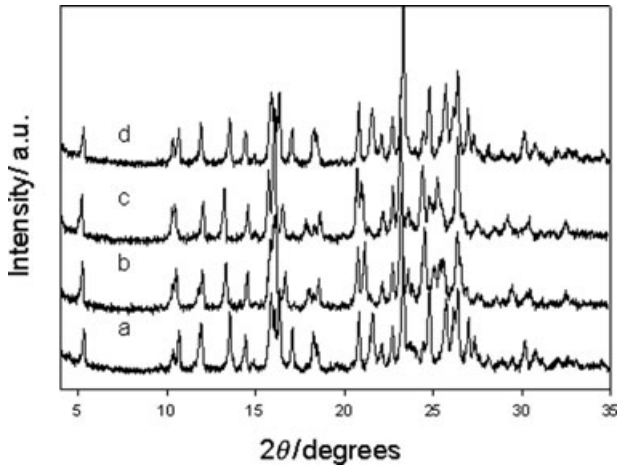

Figure 7. X-ray powder diffraction patterns of ethyl acetate–nicergoline sample collected at (a) room temperature (RT), (b) 110°C, (c) 130°C, and (d) RT after spontaneous cooling.

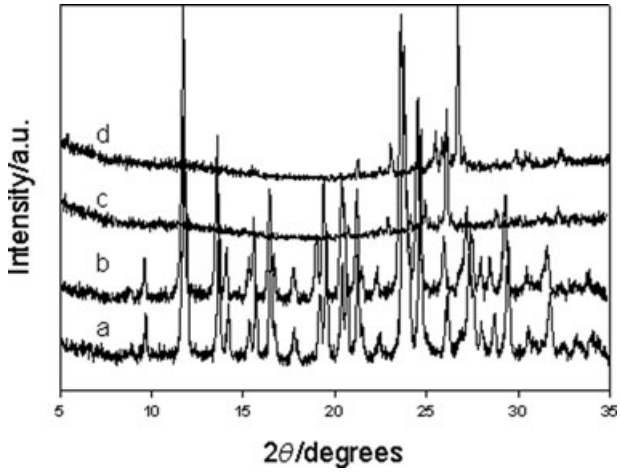

Figure 9. X-ray powder diffraction patterns of tetrahydrofurane–nicergoline sample collected at (a) room temperature (RT), (b) 110°C, (c) 130°C, and (d) RT after spontaneous cooling.

(0.1 N) was experimentally determined at different temperatures and results are given in Figure 11, wherein solubility data are plotted according to the van't Hoff equation. After equilibration, XRPD did not show changes in crystalline forms of original particles. The solubility of form II was always higher than that of form I in the temperature interval considered for this study, whatever the solvent used. The two straight lines both in water and HCl are almost parallel over the temperature range of interest and the two forms can be considered related by a monotropic relationship.[24–26]

In Figure 12, the cumulative drug releases of NIC polymorphs in water and HCl (0.1 N) were plotted versus time. The ANOVA revealed that cumulative drug releases were significantly different (significance level $p < 0.05$). Cumulative drug releases in HCl (0.1 N) were always higher than those in water, in agreement with the results of drug solubility. In addition, the form II always exhibited the highest cumulative drug release, whatever the media used. The slopes of the straight lines determined by fitting the points of each curve were used to calculate the IDRs (Table 3), which were higher for the polymorph II, whatever the media used.

The results of solubility and IDRs are very important because they suggest that the polymorphic form II could be introduced into NIC formulations in order to improve the drug bioavailability.

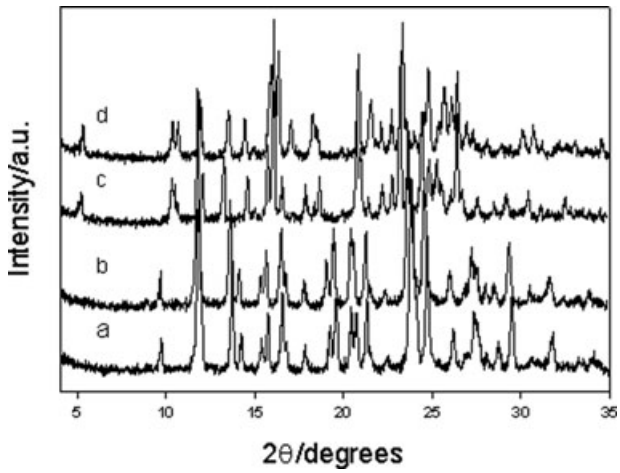

Figure 8. X-ray powder diffraction patterns of acetonitrile–nicergoline sample collected at (a) room temperature (RT), (b) 110°C, (c) 130°C, and (d) RT after spontaneous cooling.

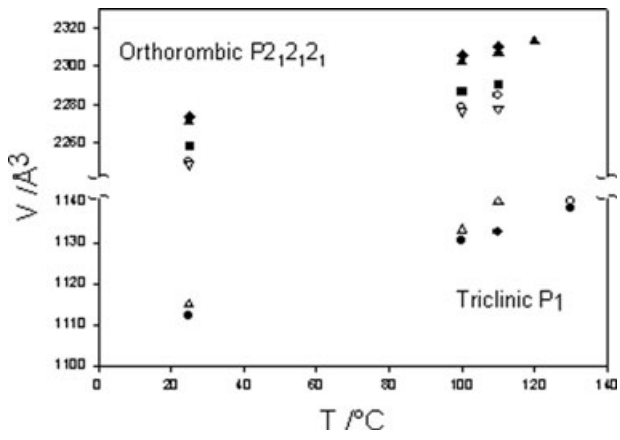

Figure 10. Temperature dependence of the cell volume for the reference–nicergoline (NIC) (△), ethyl acetate–NIC (●), acetonitrile–NIC (○), tetrahydrofurane–NIC (▲), ethanol–NIC (■), dichloromethane–NIC (◆), and acetone–NIC (▽).

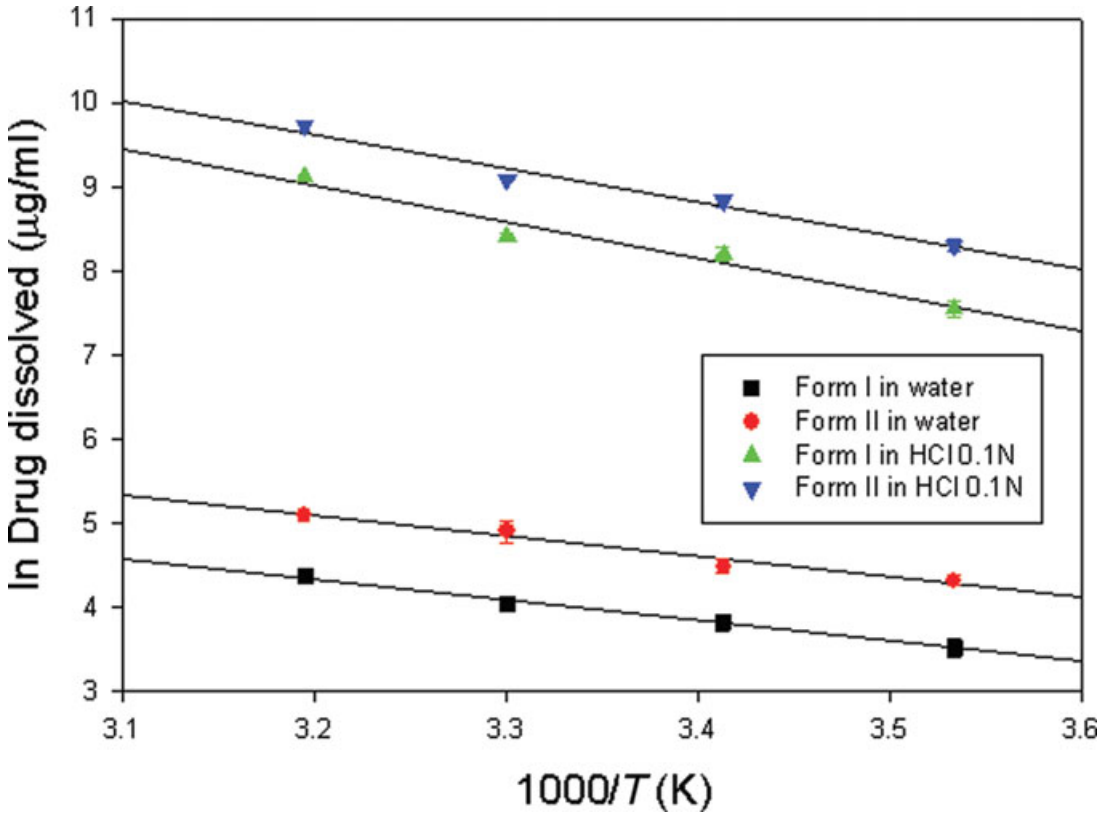

Figure 11. van't Hoff plot from the solubility data determined at different temperatures for form I [reference–nicergoline (NIC)] and form II (ethanol–NIC).

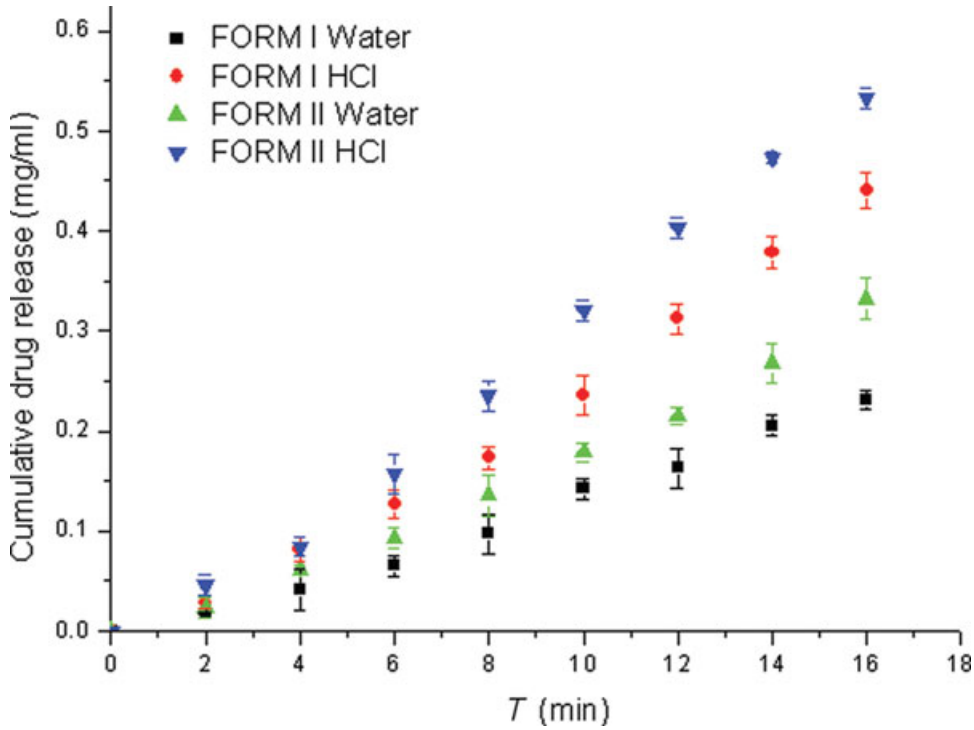

Figure 12. Cumulative drug release of nicergoline (NIC) polymorphs (form I, reference–NIC; form II, ethanol–NIC) expressed versus time in water and HCl (0.1 N).

 DOI 10.1002/jps

Table 3. Intrinsic Dissolution Rates of Nicergoline Polymorphs in Different Media

	Slope mg/(mL min)	R	IDR mol/(min mm^2)
Form I in water	0.0151	0.9948	2.3484×10^{-7}
Form II in water	0.0205	0.9935	3.1835×10^{-7}
Form I in HCl (0.1 N)	0.0282	0.9939	4.3857×10^{-7}
Form II in HCl (0.1 N)	0.0351	0.9955	5.4604×10^{-7}

Thermodynamic Relationship Between the Crystal Phases

According to the results of this study, it is possible to evaluate the thermodynamic relationship between the two polymorphic forms of NIC, using Burger–Ramberger's rules.[23]

The DSC studies never revealed transition from form II to form I. Actually, whatever the form II sample and heating rate, it melted without transition to form I, and form I crystallized from the melt. Thus, presumably the transition from form II to form I occurs at temperatures higher than the melting temperature of form I, as also suggested by the van't Hoff plot of solubility data.[24–26] For this reason, it was impossible to establish whether the transition is exothermic or endothermic, or whether it is reversible or irreversible. For the same reason, form I always appeared to be the most stable form. The enthalpy of melting endotherm of form I seemed to be slightly higher than that of form II (DHI > DHII). Solubility studies clearly showed that form II was always the most soluble, and the density of form I was higher than that of form II. From these considerations, it is possible to conclude that the thermodynamic relationship between forms I and II of NIC is monotropic.

CONCLUSIONS

The combined use of thermal, spectroscopic, and structural techniques allowed us to completely characterize the structure and thermal stability of the NIC compound.

Two NIC polymorphic crystalline forms can be stabilized depending on the crystallization solvent. Polymorph I (triclinic, $P1$ s.g.), obtained from crystallization in ETA, is stable up to its melting temperature of 134°C. This form is also present in the native NIC. Polymorph II (orthorhombic, $P2_12_12_1$ s.g.), obtained from crystallization by other solvents, shows a peculiar behavior with temperature. It melts at about 120°C–122°C, and then depending on the sample and heating rate, it can recrystallize to form I as evidenced also by DSC performed at low heating rate (1°C/min).

Solubility and IDRs performed in distilled water and in 0.1 N HCl solutions showed higher values for the orthorhombic form. This suggests that polymorph II would be more suitable for pharmaceutical applications.

In addition, the analysis of the results previously discussed and the application of Burger–Ramberger's rules allow to ascertain a monotropic thermodynamic relationship between forms I and II.

ACKNOWLEDGMENTS

The authors would like to thank Sheila Beatty for her linguistic revision of this text.

REFERENCES

1. Amidon GL, Lennernäs H, Shah VP, Crison JR. 1995. A theoretical basis for a biopharmaceutical drug classification: The correlation of in vitro drug product dissolution and in vivo bioavailability. Pharm Res 12:413–420.
2. Leuner C, Dressman J. 2000. Improving drug solubility for oral delivery using solid dispersions. Eur J Pharm Biopharm 50:47–60.
3. Lipinski C. 2001. Poor aqueous solubility—An industry wide problem in drug delivery. Am Pharm Rev 5:82–85.
4. Al-Saieq SS, Riley GS. 1982. Polymorphism in sulphonylurea hypoglycaemic agents: II. Chlorpropamide. Pharm Acta Helv 57:8–11.
5. Haleblian J, McCrone W. 1969. Pharmaceutical applications of polymorphism. J Pharm Sci 58:911–929.
6. Hörter D, Dressman JB. 1997. Influence of physicochemical properties on dissolution of drugs in the gastrointestinal tract. Adv Drug Del Rev 25:3–14.
7. Khankari RK, Grant DJW. 1995. Pharmaceutical hydrates. Thermochim Acta 248:61–79.
8. Chawla G, Bansal AK. 2007. A comparative assessment of solubility advantage from glassy and crystalline forms of a water-insoluble drug. Eur J Pharm Sci 32:45–57.
9. Woodcock BG, Acerbi D, Merz PG, Rietbrock S, Rietbrock N. 1993. Supermolecular inclusion of piroxicam with β-cyclodextrin: Pharmacokinetic properties in man. Eur J Rheumatol Inflamm 12:12–28.
10. Miyayi T, Inoue Y, Acarturk F, Imai T, Otagiri M, Uekama K. 1992. Improvement of oral bioavailability of fenbufen by cyclodextrin complexations. Acta Pharm Nord 4:17–22.
11. Verheven S, Blaton N, Kinget R, Van Den Mooter G. 2002. Mechanism of increased dissolution of diazepam and temazepam from polyethylene glycol 6000 solid dispersions. Int J Pharm 249:45–58.
12. Heitz C, Descombes JJ, Miller RC, Stoclet JC. 1986. α-Adrenoceptor antagonistic and calcium antagonistic effects of nicergoline in the rat isolated aorta. Eur J Pharmacol 123:279–285.
13. Brossi A. 1990. The alkaloids. Chemistry and pharmacology. Vol. 38. San Diego, California: Academic Press Inc., p 142.
14. Venn RD. 1980. Review of clinical studies with ergots in gerontology. In: Ergot compounds and brain function; Goldstein M, Liberman A, Calne DB, Thorner MO, Eds. New York: Raven Press, pp 363–377.
15. Goo D, Palosi E, Szporny L. 1988. Comparison of the effects of vinpocetine, vincamine, and nicergoline on the normal and hypoxia-damaged learning process in spontaneously hypertensive rats. Drug Dev Res 15:75–85.
16. Pastoris O, Vercesi L, Allorio F, Dossena M. 1988. Effect of hypoxia, aging and pharmacological treatment on muscular metabolites and enzyme activities. Farmaco Sci 43:627–642.

17. Triulzi E, Devizzi S, Margonato A. 1981. Use of nicergoline in acute myocardial infarction with diastolic hypertension. Farmaco Prat 36:449–455.
18. Hušák M, Had J, Kratochvíl B, Cvak L, Stuchlík J, Jegorov A. 1994. X-ray absolute structure of nicergoline (form I). Quantitative analysis of nicergoline phase mixture: FormI/form II. Coll Czech Chem Commun 59:1624–1636.
19. Husàk M, Kratochvil B, Ondraček J, Maixner J, Jerolov A, Stuchlik J. 1994. The crystal and absolute molecular structure od "low melting" nicergoline (form II). Z Kristallogr 209:260–262.
20. Foresti E, Sabatino P, Riva di Sanseverino L, Fusco R, Tosi C, Tonani R. 1988. Structure and molecular orbital study of ergoline derivatives. 1-(6-Methyl-8β-ergolinylmethyl)-imidazolidine-2,4-dione (I) and 2-(10-methoxy-1,6-dimethyl-8β-ergolinyl)ethyl 3,5-dimethyl-1H-2-pyrrolecarboxylate toluene hemisolvate (II) and comparison with nicergoline (III). Acta Cryst B44:307–315.
21. Bruker AXS. 2005. TOPAS V3.0: General profile and structural analysis software for powder diffraction data. User Manual Bruker AXS, Karlsruhe, Germany.
22. Banakar UV. 1992. Pharmaceutical dissolution testing. In: Swarbrick J. Ed., New York: Marcel Dekker, pp 55–105.
23. Burger A, Ramberger R. 1979. On the polymorphism of pharmaceuticals and other molecular crystals. I. Theory of thermodynamic rules. Mikrochim Acta 2:259–271.
24. Li H, Kiang Y-H, Jona J. 2009. Multiple approaches to pharmaceutical polymorphism investigation—A case study. Eur J Pharm Sci 38:426–432.
25. Yang X, Wang X, Ching CB. 2008. Solubility of form α and form γ of glycine in aqueous solutions. J Chem Eng Data 53:1133–1137.
26. Nordstrom FL, Rasmuson AC. 2006. Polymorphism and thermodynamics of m-hydroxybenzoic acid. Eur J Pharm Sci 28:377–384.